Article

Dusty Common Envelope Evolution

Lionel Siess [1,*](ID), Luis C. Bermúdez-Bustamante [2,3](ID), Orsola De Marco [2,3](ID), Daniel J. Price [4](ID), Miguel González-Bolívar [2,3](ID), Chunliang Mu [2,3](ID), Mike Y. M. Lau [4,5,6](ID), Ryosuke Hirai [4,5,7](ID) and Taïssa Danilovich [4,8,9](ID)

1   Institut d'Astronomie et d'Astrophysique, Université Libre de Bruxelles (ULB), CP 226, 1050 Brussels, Belgium
2   School of Mathematical and Physical Sciences, Macquarie University, Balaclava Road, North Ryde, Sydney, NSW 2109, Australia; luiscarlos.bermudez@mq.edu.au (L.C.B.-B.); orsola.demarco@mq.edu.au (O.D.M.); miguel-angel.gonzalez-boliv@hdr.mq.edu.au (M.G.-B.); chunliang.mu@hdr.mq.edu.au (C.M.)
3   Astrophysics and Space Technologies Research Centre, Macquarie University, Balaclava Road, North Ryde, Sydney, NSW 2109, Australia
4   School of Physics and Astronomy, Monash University, Clayton, VIC 3800, Australia; daniel.price@monash.edu (D.J.P.); mike.lau@h-its.org (M.Y.M.L.); ryosuke.hirai@monash.edu (R.H.); taissa.danilovich@monash.edu (T.D.)
5   OzGrav: The ARC Centre of Excellence for Gravitational Wave Discovery, Hawthorn, VIC 3122, Australia
6   Heidelberger Institut für Theoretische Studien, Schloss-Wolfsbrunnenweg 35, 69118 Heidelberg, Germany
7   Astrophysical Big Bang Laboratory (ABBL), Cluster for Pioneering Research, RIKEN, Wako 351-0198, Saitama, Japan
8   ARC Centre of Excellence for All Sky Astrophysics in 3 Dimensions (ASTRO 3D), Clayton, VIC 3800, Australia
9   Institute of Astronomy, KU Leuven, Celestijnenlaan 200D, 3001 Leuven, Belgium
*   Correspondence: lionel.siess@ulb.be

Abstract: We present the first hydrodynamical simulations of common envelope evolution that include the formation of dust and the effect of radiation pressure on dust grains. We performed smoothed particle hydrodynamics simulations of the CE evolution for two systems made of a 1.7 $M_\odot$ and 3.7 $M_\odot$ AGB star primary with a 0.6 $M_\odot$ binary companion. The results of our calculations indicate that dust formation has a negligible impact on the gas dynamics essentially because dust forms in the already unbound material. The expansion and cooling of the envelope yield very early and highly efficient production of dust. In our formalism, which does not consider dust destruction, almost 100% of the available carbon that is not locked in CO condensates in dust grains. This massive dust production, thus, strongly depends on the envelope mass and composition, in particular, its C/O ratio, and has a considerable impact on the observational aspect of the object, resulting in a photospheric radius that is approximatively one order of magnitude larger than that of a non-dusty system.

Keywords: stars; AGB; post-AGB; winds; outflows; binaries

1. Introduction

Common envelope (CE) evolution is a critical phase in the evolution of binary systems and a pathway to the formation of various astrophysical phenomena, including compact binaries, type Ia supernovae, cataclysmic variables, or X-ray binaries. During CE evolution, one star in a binary system expands to the point where it engulfs its companion, leading to a shared envelope that enshrouds both cores. The subsequent interaction and eventual ejection of this envelope can significantly alter the orbital parameters of the system, often resulting in a dramatic reduction in the orbital separation [1].

The CE phase evolution involves different stages [2]. Initially, as the primary star expands and engulfs its companion, the binary system loses corotation due to the interaction between the stellar components. The friction causes the in-spiral and deposition of both orbital energy and angular momentum in the envelope. Depending on the initial parameters

(the separation and evolutionary status of the primary), the end product is either a close binary system if the envelope is efficiently ejected or the merger of the two stars.

Advancements in numerical simulations have begun to shed light on the dynamical processes occurring during CE phases. Hydrodynamic simulations (for a recent review, see, e.g., [3]) have provided detailed views of the envelope's response to the embedded binary, revealing the complex interplay between drag forces, heating, and envelope ejection [4,5] and the key role of recombination energy in assisting the envelope ejection [6].

Dust formation is likely to occur in the cool, dense regions of the envelope, particularly in cases involving evolved stars such as asymptotic giant branch (AGB) stars. The radiation pressure exerted on dust grains can provide an additional acceleration, thereby aiding the ejection of the envelope. Moreover, dust opacity increases the envelope's optical depth, affecting the appearance of the star.

Earlier studies investigating the role of dust in interacting binary stars focused on the pre-common envelope phase [7], used post-processing methods to estimate dust formation from the 3D simulations [8,9], or tried to assess the role of radiation pressure on dust in the envelope ejection [10].

In this work, we report on our recent smoothed particle hydrodynamics (SPH) simulations of common envelope evolution, including the treatment of dust following the works of [11,12]. The implementation of dust is described in Section 2, and the initial setup is presented in Section 2. In Section 3, we discuss our results and summarize our key results.

2. Dust Production

Dust formation involves the initial aggregation of gas-phase atoms and molecules into small clusters, which then grow into solid dust grains. This process typically begins with the formation of stable seed nuclei, often composed of refractory elements such as carbon, silicon, or titanium [13]. Once these nuclei form, they act as condensation centers for additional material, allowing the grains to grow through accretion. The efficiency of nucleation and subsequent dust growth depend on local conditions, including temperature, density, and chemical composition. For instance, in the atmospheres of asymptotic giant branch (AGB) stars, carbon-rich or oxygen-rich environments favor the formation of different types of dust, such as amorphous carbon or silicates, respectively [14]. In our simulation, nucleation and dust growth are calculated using the theory of moments developed by Gail and Sedlmayr [13,15]. The main idea is not to follow the evolution of the grain size distribution $f(N, t)$ but, instead, its moments $\mathcal{K}_i$, defined as

$$\mathcal{K}_i = \sum_{N=N_l}^{\infty} N^{i/3} f(N, t), \tag{1}$$

where N is the number of monomers (dust building blocks) in a grain and $N_l \sim 1000$ is the minimum number of monomers that a cluster must contain to be considered a dust grain. We consider C-rich chemistry (i.e., with a carbon-to-oxygen (C/O) ratio > 1) and heterogeneous nucleation. In this framework, a grain can grow by the addition of C, C_2, C_2H, and C_2H_2. To estimate the abundance of the monomers, a small chemical network including 7 atoms and 25 molecules is solved at each time step, assuming the chemistry is at equilibrium. Departure from chemical equilibrium could be induced by the passage of a shock wave, which can dissociate molecules, or by the photo-dissociation of atoms and molecules by a UV flux. In the dense inner regions of the outflow where dust forms, chemical equilibrium is expected to prevail in the absence of strong chromospheric UV emission (see, e.g., Chap 15.3.2 of [13]). The derived abundances of monomers then allow for calculating the nucleation and growth rates needed to evolve the moments (for details, see [16]).

One of the benefits of this theory is to relate the various moments to fundamental dust parameters, which include the following:

(a) The mean grain density $n_d = \mathcal{K}_0$; that is, the density of all dust grains with size $N \geq N_l$.

(b) The average grain radius $\langle a \rangle = a_0 \mathcal{K}_1 / \mathcal{K}_0$, where a_0 is the size of the carbon atom;

(c) The average grain surface $\langle A_N \rangle = 4\pi a_0^2 \mathcal{K}_2 / \mathcal{K}_0$;

(d) The average particle size $\langle N \rangle = \mathcal{K}_3 / \mathcal{K}_0$;

(e) The number density of monomers of size $N \geq N_l$ condensed into grains $n_{\text{cond}} = \mathcal{K}_3$.

Provided the grain size is smaller than the wavelength of the peak stellar radiation, i.e., in the regime of the small particle limit, the third moment $\mathcal{K}_3$ can be shown to be directly proportional to the dust opacity. For an AGB star of ≈2500 K, the maximum flux is produced around $\lambda_{\text{max}} \approx 1$ μm, which sets the maximum size of the dust grain. We also stress that, in our formalism, dust destruction is not accounted for, meaning that carbon abundance always decreases as dust grows.

In this study, we also considered a simple analytical expression for dust opacity κ_{dust}, initially devised by Bowen [17] to simulate dust-driven wind, the expression of which is given by

$$\kappa_{\text{dust}} = \frac{\kappa_{\text{max}}}{1 + e^{(T - T_{\text{cond}})/\delta}} \tag{2}$$

where κ_{max} is the maximum dust opacity, T_{cond} is the condensation temperature of the dust (around 1500 K for C-rich compositions), and $\delta \approx 100$ K is the temperature range over which dust condensates (see [11] for details).

Once the dust opacity κ_{dust} is calculated, using either the theory of moments or the Bowen expression, the effect of dust on the hydrodynamics can be accounted for by including a radiative acceleration term in the equation of motion

$$\frac{d\mathbf{v}}{dt} = -\frac{\nabla P}{\rho} - \nabla \phi_{\text{gas}-\text{gas}} - \nabla \phi_{\text{sink}-\text{gas}} + \frac{(\kappa_{\text{dust}} + \kappa_{\text{gas}})L}{4\pi r^2 c} \frac{\mathbf{r}}{r} \tag{3}$$

where P is the pressure, ρ is the density, $\phi_{\text{gas}-\text{gas}}$ and $\phi_{\text{sink}-\text{gas}}$ are the gravitational potentials from the SPH particles (self-gravity) and between a particle and the sink masses, respectively. As will be described in the next section, the AGB core and stellar companion companion are modeled as two separate sink particles, characterized by their mass and accretion radius among other properties. The radius r is the distance from the AGB core, which is assumed to produce a constant luminosity L. We assume a constant gas opacity $\kappa_{\text{gas}} = 2 \times 10^{-4}$ cm^2 g^{-1}, as proposed by [17], which is a good approximation for the opacity surrounding a typical C-rich AGB star (for details, see [16]).

Initial Setup

The hydrodynamical simulations are performed with the smoothed particle hydrodynamics code Phantom [18]. We use Phantom's implementation of MESA's OPAL/SCVH EoS to account for recombination energy (as conducted by [6]) and consider two initial stellar models: 1.7 $M_\odot$ and 3.7 $M_\odot$ solar metallicity AGB stars with core masses of 0.56 $M_\odot$ and 0.72 $M_\odot$ and radii 260 $R_\odot$ and 343 $R_\odot$, respectively. The stellar models were relaxed from 1D MESA models [19] using the procedure described in [20]. The stellar core was excised and replaced by a sink particle of the same mass. The companion star is modeled as a sink particle of 0.6 $M_\odot$ and could represent a low-mass main sequence star or a white dwarf. The simulation includes 1.37×10^6 particles, and a C/O ratio of 2.5 is assumed.

3. Results

3.1. Orbital Evolution and Mass Unbinding

In all our simulations, the in-spiral ends around 7.5 years (Figure 1). The inclusion of dust nucleation (solid blue line) hastens the plug in and leads to slightly larger final separations. The shortening of the in-spiral phase is attributed to an earlier expansion of the envelope in the dusty simulations. As will be discussed in Section 3.2, dust forms very quickly, and the radiative acceleration gives the particles extra momentum, so they have

slightly higher velocities than in a non-dusty simulation. Because of this faster ejection, the companion stalls at a slightly larger orbital separation.
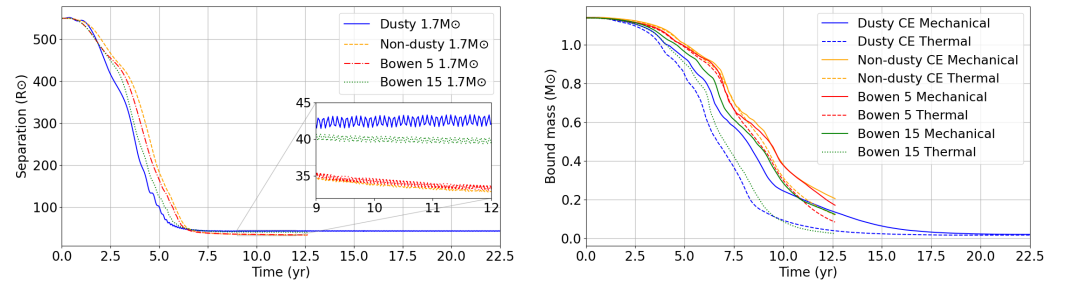

Figure 1. Evolution of the separation (**left**) and bound mass (**right**) in the 1.7 $M_\odot$ model for different dust implementations based on the nucleation model (dusty), the absence of dust (non-dusty), or the Bowen model with two values of $\kappa_{max} = 5$ and 15 cm^2 g^{-1}. For the estimate of the bound mass, we consider the two definitions of the total energy: the mechanical one associated with E_{tot}^{m} and the thermal one linked to E_{tot}^{th}.

The total energy of a particle can be defined as the sum of its kinetic and gravitational potential energies, given by the equation $E_{tot}^{m} = E_{kin} + E_{gr}$. The thermal contribution E_{th} can also be included in this definition, yielding total energy as $E_{tot}^{th} = E_{kin} + E_{gr} + E_{th}$. It should be noted that in this latter expression, recombination energy is not considered as it is still debated what fraction can be radiated away [21,22]. The bound mass is then calculated by summing the contribution from all the particles that have $E_{tot} < 0$. The results (right panel of Figure 1) show that the envelope gets unbound more rapidly in the nucleation calculations (blue lines vs. yellow lines) but, in the end, dust does not increase mass ejection significantly (the non-dusty simulations stopped earlier at a higher bound mass, but the curves show the same tendency to converge toward an almost complete unbinding of the envelope). The Bowen dust simulations with $\kappa_{max} = 5$ cm^2 g^{-1} in Equation (2) behave very similar to the non-dusty simulations, but when $\kappa_{max} = 15$ cm^2 g^{-1}, the evolution is very comparable to the nucleation case, except that the envelope is expelled slightly more rapidly. We also notice that in our simulations, the final unbound mass weakly depends on the assumed criterion (E_{tot}^{m} or E_{tot}^{th}).

3.2. Dust Formation and Properties

The left panel of Figure 2 shows, as a function of distance from the AGB star, the total energy of the particles when the dust starts forming efficiently. We arbitrarily trace this moment by selecting the particles when the dust opacity reaches $\kappa_{dust} = 0.02$ cm^{2}g^{-1} (the distribution of particles in this plot is weakly dependent on this threshold opacity). As can be seen, the total particle's energy is always positive, indicating that dust is forming in the unbound material. This explains why dust has such a small effect on the unbound mass (Figure 1). The color of the particles refers to the time of dust nucleation in years (t_{nuc}). Initially, dust forms in the inner region (yellow color), and by the end of the simulation, it is active through almost the entire envelope (up to ∼200 au). Dust forms as early as 1 year from the onset of the simulation and occurs preferentially in a shell that expands, grows thicker, and becomes more symmetric. Movies illustrating the evolution of the structure and of various quantities can be found at (accessed 21 November 2024) https://tinyurl.com/y455avdj. The opacity in the shell increases and by the end of the in-spiral phase, reaches a maximum of around $\kappa_{dust} \approx 20$ cm^{2}g^{-1} (Figure 2, right), making it optically thick (see Section 3.3). We also note that contrary to the 3.7 $M_\odot$ model, the shell in the 1.7 $M_\odot$ model is slightly elongated in the polar direction. This is likely related to the different mass ratios and initial separation. More details about the evolution of the dust properties can be found in [12].
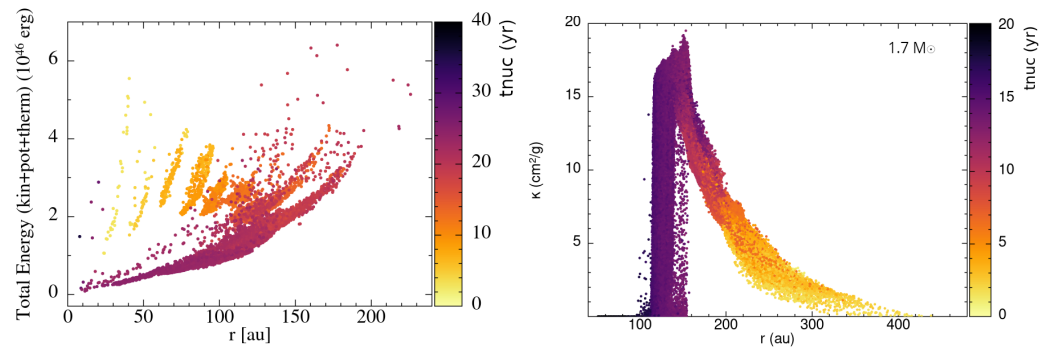
Figure 2. (**Left**) Energy and position of the particles in the 1.7 $M_\odot$ model when the dust opacity first reaches $\kappa_{\rm dust} = 0.02$ cm^{2}g^{-1}. (**Right**) Dust opacity as a function of distance after 20 years of simulation. The color bar indicates $t_{\rm nuc}$, i.e., the time in years since the beginning of the simulation when the opacity first reaches $\kappa_{\rm dust} = 0.02$ cm^{2}g^{-1}. Particles that form dust early are located in the inner region (left panel), but after 20 years, they have traveled to the outer region of the simulation (right panel). A movie of the evolution of κ (right panel) is available at the following URL: https://tinyurl.com/bd3ae6cc (accessed 21 November 2024).

The left panel of Figure 3 shows the particles' average dust grain size as a function of distance from the AGB core at the end of the simulation. The most remote particles, where dust first formed (yellow points with lower $t_{\rm nuc}$), contain relatively small grains with sizes ranging between $\sim$0.02 μm and 0.06 μm. With increasing time, dust growth proceeds and grains reach a maximum size of $\sim$1 μm around $t_{\rm nuc} \sim 12$ years. By the end of the simulation, nucleation is still active in the inner region where the density is high enough for monomers to accumulate on the seed particles. Since dust forms in the unbound material are at a relatively large distance ($\gtrsim$10 au) from the central core, the radiative acceleration has a weak impact on the flow, the evolution of which is mainly controlled by the deposition and transport of the orbital energy.
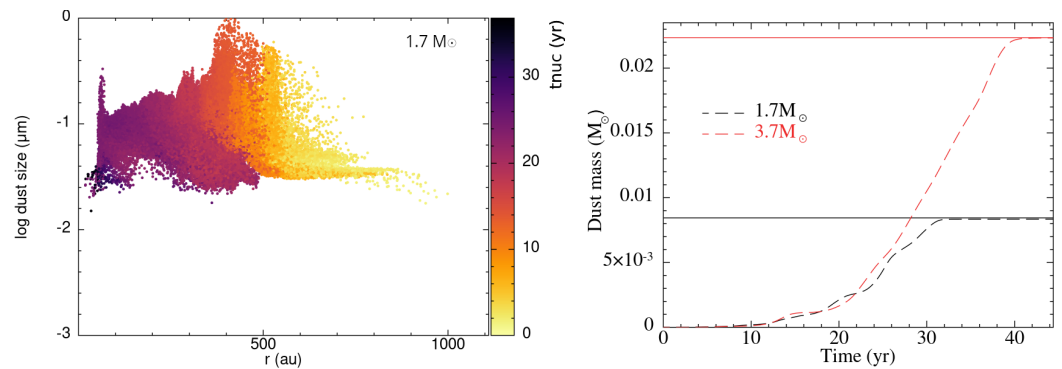

Figure 3. (**Left**) Average particle's grain size as a function of distance at the end of the simulation (after $\sim$40 years) for the 1.7 $M_\odot$ model. (**Right**) Dust mass as a function of time for the 1.7 and 3.7 $M_\odot$ models. The horizontal lines indicate the maximum possible dust production, which depends on the initial C/O ratio and envelope mass.

Dust production is very efficient during the CE evolution and really starts after $\sim$10–12 years (right panel of Figure 3). Within $\sim$32 years (38 years), a plateau is reached in the 1.7 (3.7) $M_\odot$ model when all the carbon that is not locked into oxygen is trapped in the grains. This massive production is a consequence of the large envelope expansion that allows the temperature to drop below the condensation value (1500 K) for nucleation to be efficient. This leads to the production of $\approx$0.8 $\times$ 10^{-2} $M_\odot$ and 2.2 $\times$ 10^{-2} $M_\odot$ of dust for the 1.7 and 3.7 $M_\odot$ model, respectively. The efficiency is close to 100%, but this is an upper limit because our models do not account for dust destruction. It should be emphasized that the amount of dust so produced strongly depends on the envelope mass and composition,

in particular, its C/O ratio. The key point is that CE evolution produces as much dust as a star during its TP-AGB phase, but it does this in only a few decades.

3.3. Photospheric Appearance

As previously mentioned, the formation of dust in the expanding envelope does not significantly impact the hydrodynamics, but it can substantially affect the appearance of the object. To estimate the photospheric radius, we performed simple inward ray tracing to determine where the optical depth first reaches $\tau = 1$. The integration is made along the x, y, and z axes and then averaged to obtain the polar (along $\pm z$) and equatorial ($\pm x$ and $\pm y$) radii. As shown in Figure 4, the photosphere initially grows more rapidly in the orbital than in the polar direction, tracing the asymmetries in the flow. By 2.5–5 years, the polar and equatorial photospheric radii become very similar, making the envelope appear roughly spherically symmetric. Without dust and with a lower mass ratio, we find that asymmetry is more pronounced. The main effect is the much larger photospheric radius of the dusty simulations, making the object appear almost ten times bigger. Our simulations do not reproduce the very non-spherical, bipolar morphology seen in central stars of planetary nebulae (CSPNe). This discrepancy arises partly because our models show that the release of recombination energy that allows dust to form produces a more spherical ejection. Additionally, we do not account for the interaction of a fast wind with the ejected envelope during the planetary phase, which has been shown to produce bipolar outflows (e.g., [23]).
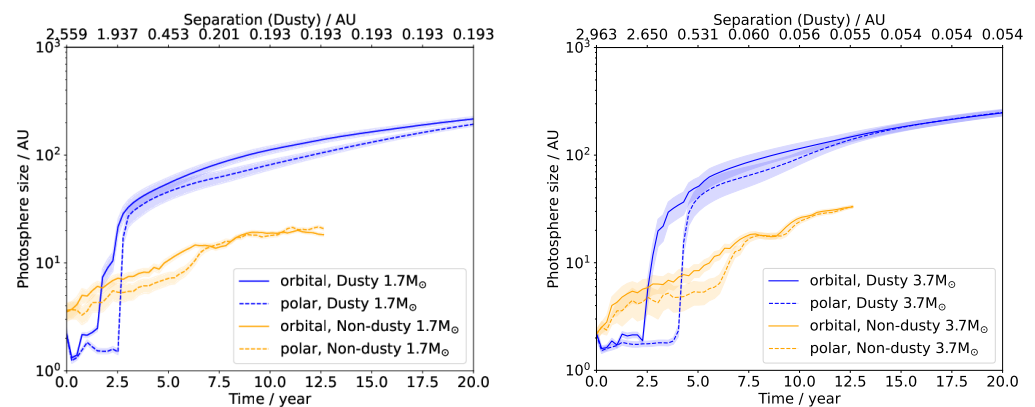

Figure 4. Evolution of the photospheric radius for the 1.7 (**left**) and 3.7 $M_\odot$ (**right**) models. The results of the dusty and non-dusty simulations are shown in blue and yellow, respectively. The mean equatorial and polar photospheric radii are shown in solid and dotted lines. The shaded region corresponds to the smoothing length and provides an estimate of the uncertainty.

4. Conclusions

Using the SPH code Phantom, we performed the first simulations of common envelope evolution, including the formation of dust, following the theory of moments developed by [15]. The main conclusions are as follows:

- Dust forms in the unbound material and does not help to unbind more mass.
- Dust forms early in the simulation (already $\sim$1 y after the start of the simulation).
- Dust formation is very efficient ($\approx 10^{-3}$–10^{-2} $M_\odot$ of dust is produced in our models). However, these mass estimates should be considered as upper values, as dust destruction is not included. However, the point is that a common envelope evolution is susceptible to producing as much dust as an AGB star but in only a few decades, as compared to tens of thousands of years of the thermally pulsing AGB duration.
- If dust is not efficiently destroyed, it will dramatically impact the optical appearance of the object, as shown by the large increase in the photospheric radius. We should also expect this source to present a strong IR excess.

Data Availability Statement: The data underlying this article will be shared on reasonable request to the corresponding author.

Conflicts of Interest: The authors declare no conflicts of interest.

References

1. Paczynski, B. Common Envelope Binaries. In *Structure and Evolution of Close Binary Systems*; Eggleton, P., Mitton, S., Whelan, J., Eds.; IAU Symposium; Springer: Berlin/Heidelberg, Germany, 1976; Volume 73, p. 75.
2. Ivanova, N.; Justham, S.; Chen, X.; De Marco, O.; Fryer, C.L.; Gaburov, E.; Ge, H.; Glebbeek, E.; Han, Z.; Li, X.D.; et al. Common envelope evolution: Where we stand and how we can move forward. *Astron. Astrophys. Rev.* **2013**, *21*, 59. [CrossRef]
3. Röpke, F.K.; De Marco, O. Simulations of common-envelope evolution in binary stellar systems: Physical models and numerical techniques. *Living Rev. Comput. Astrophys.* **2023**, *9*, 2. [CrossRef]
4. Ricker, P.M.; Taam, R.E. An AMR Study of the Common-envelope Phase of Binary Evolution. *Astrophys. J.* **2012**, *746*, 74. [CrossRef]
5. Ohlmann, S.T.; Röpke, F.K.; Pakmor, R.; Springel, V.; Müller, E. Magnetic field amplification during the common envelope phase. *Mon. Not. R. Astron. Soc.* **2016**, *462*, L121–L125. [CrossRef]
6. Reichardt, T.A.; De Marco, O.; Iaconi, R.; Chamandy, L.; Price, D.J. The impact of recombination energy on simulations of the common-envelope binary interaction. *Mon. Not. R. Astron. Soc.* **2020**, *494*, 5333–5349. [CrossRef]
7. Bermúdez-Bustamante, L.C.; García-Segura, G.; Steffen, W.; Sabin, L. AGB winds in interacting binary stars. *Mon. Not. R. Astron. Soc.* **2020**, *493*, 2606–2617. [CrossRef]
8. Iaconi, R.; Maeda, K.; De Marco, O.; Nozawa, T.; Reichardt, T. Properties of the post-inspiral common envelope ejecta—I. Dynamical and thermal evolution. *Mon. Not. R. Astron. Soc.* **2019**, *489*, 3334–3350. [CrossRef]
9. Iaconi, R.; Maeda, K.; Nozawa, T.; De Marco, O.; Reichardt, T. Properties of the post in-spiral common envelope ejecta II: Dust formation. *Mon. Not. R. Astron. Soc.* **2020**, *497*, 3166–3179. [CrossRef]
10. Glanz, H.; Perets, H.B. Efficient common-envelope ejection through dust-driven winds. *Mon. Not. R. Astron. Soc.* **2018**, *478*, L12–L17. [CrossRef]
11. González-Bolívar, M.; Bermúdez-Bustamante, L.C.; De Marco, O.; Siess, L.; Price, D.J.; Kasliwal, M. Dust Formation in Common Envelope Binary Interaction—I: 3D Simulations Using the Bowen Approximation. *arXiv* **2023**, arXiv:2306.16609. [CrossRef]
12. Bermúdez-Bustamante, L.C.; De Marco, O.; Siess, L.; Price, D.J.; González-Bolívar, M.; Lau, M.Y.M.; Mu, C.; Hirai, R.; Danilovich, T.; Kasliwal, M.M. Dust formation in common envelope binary interactions—II: 3D simulations with self-consistent dust formation. *Mon. Not. R. Astron. Soc.* **2024**, *533*, 464–481. [CrossRef]
13. Gail, H.P.; Sedlmayr, E. *Physics and Chemistry of Circumstellar Dust Shells*; Cambridge University Press: Cambridge, UK, 2013.
14. Höfner, S.; Olofsson, H. Mass loss of stars on the asymptotic giant branch. Mechanisms, models and measurements. *Astron. Astrophys. Rev.* **2018**, *26*, 1. [CrossRef]
15. Gail, H.P.; Keller, R.; Sedlmayr, E. Dust formation in stellar winds. I—A rapid computational method and application to graphite condensation. *Astron. Astrophys.* **1984**, *133*, 320–332.
16. Siess, L.; Homan, W.; Toupin, S.; Price, D.J. 3D simulations of AGB stellar winds. I. Steady winds and dust formation. *Astron. Astrophys.* **2022**, *667*, A75. [CrossRef]
17. Bowen, G. Dynamical modeling of long-period variable star atmospheres. *Astrophys. J.* **1988**, *329*, 299–317. [CrossRef]

18. Price, D.J.; Wurster, J.; Tricco, T.S.; Nixon, C.; Toupin, S.; Pettitt, A.; Chan, C.; Mentiplay, D.; Laibe, G.; Glover, S.; et al. Phantom: A Smoothed Particle Hydrodynamics and Magnetohydrodynamics Code for Astrophysics. *Publ. Astron. Soc. Aust.* **2018**, *35*, e031. [CrossRef]
19. Paxton, B.; Bildsten, L.; Dotter, A.; Herwig, F.; Lesaffre, P.; Timmes, F. Modules for experiments in stellar astrophysics (MESA). *Astrophys. J. Suppl. Ser.* **2011**, *192*, 3. [CrossRef]
20. Gonzalez-Bolivar, M.; De Marco, O.; Lau, M.Y.; Hirai, R.; Price, D.J. Common envelope binary interaction simulations between a thermally-pulsating AGB star and a low mass companion. *arXiv* **2022**, arXiv:2205.09749. [CrossRef]
21. Soker, N.; Grichener, A.; Sabach, E. Radiating the Hydrogen Recombination Energy during Common Envelope Evolution. *Astrophys. J. Lett.* **2018**, *863*, L14. [CrossRef]
22. Grichener, A.; Sabach, E.; Soker, N. The limited role of recombination energy in common envelope removal. *Mon. Not. R. Astron. Soc.* **2018**, *478*, 1818–1824. [CrossRef]
23. Frank, A.; Chen, Z.; Reichardt, T.; De Marco, O.; Blackman, E.; Nordhaus, J. Planetary Nebulae Shaped by Common Envelope Evolution. *Galaxies* **2018**, *6*, 113. [CrossRef]